Materials Advances

ROYAL SOCIETY OF CHEMISTRY

PAPER

View Article Online
View Journal | View Issue

Cite this: *Mater. Adv.*, 2022, 3, 8629

Highly stable and water dispersible polymer-coated $CsPbBr_3$ nanocrystals for Cu-ion detection in water†

Manav Raj Kar, Urjjarani Patel and Saikat Bhaumik *

Recently, $CsPbX_3$ (X = I, Br, Cl) nanocrystals (NCs) have shown huge potential in the fields of various optoelectronic applications. However, the $CsPbX_3$ NCs degrade very rapidly in the presence of water and heat, because of dynamic oleic acid and oleylamine capping ligands. The silica-coated $CsPbBr_3$ NCs are comparatively stable but the synthesis is slightly complicated and needs several hours to complete the reaction process. These silica-coated NCs also tend to agglomerate among themselves, which is unfavorable for display technologies and bioimaging applications. In these regards, we introduce novel polymers [polyvinylpyrrolidone and *n*-isopropyl acrylamide] along with oleic acid and oleylamine that are encapsulated around the $CsPbBr_3$ NCs during the synthesis procedure at room temperature. Such NCs are highly luminescent in the green spectral region with a maximum photoluminescence quantum yield of up to 93%, have narrower emission spectra, and can easily disperse in water. The size distribution of the polymer-coated NCs becomes more uniform and well-dispersed. The water dispersity and stability of these polymer-coated NCs significantly improved in comparison to the conventional silica-coated NCs. Such water-stable NCs were tested as a luminescent probe for Cu^{2+}-ion detection in water that shows a detection limit of 18.6 μM. These outcomes are very encouraging for futuristic display technologies, bioimaging, and sensing applications.

Received 21st June 2022,
Accepted 11th September 2022

DOI: 10.1039/d2ma00719c

rsc.li/materials-advances

Introduction

In the past few years, $CsPbX_3$ (X = I, Br, Cl) nanocrystals (NCs) have been extensively employed in the fabrication of different optoelectronic devices due to some of their excellent inherent properties, such as their high absorption coefficient, color-tunable emission spectra, high photoluminescence quantum yield (PLQY), narrow full width at half maximum (FWHM), better color purity, easy solution processability, and so on.[1–8] The hot-injection synthesis of cubic-shaped $CsPbX_3$ NCs was first introduced by Protesescu *et al.*[9] However, it's very challenging to synthesize phase pure $CsPbX_3$ NCs at room temperature since some unwanted perovskite crystal phases (*i.e.*, Cs_4PbBr_6, $CsPb_2Br_5$) are also formed, which overall reduces the NCs quality and emission intensity.[10–12] Nowadays, various synthesis methods are adopted to further improve the NCs crystallinity; controlling the shape, size and composition; color tunability; enhancement of PL intensity and stability.[1,2,13–15] Narrow emission linewidth from the light sources is desirable for improving color metrics in lighting and better color gamut for displays,[9,16,17] and also beneficial for sensing applications due to high signal to noise ratio for detection.[18–20] In recent times, many different NCs have evolved as promising materials for disease diagnostics and therapeutics.[21,22] The definite size, shape, and/or surface chemistry of the NCs exhibit their specific functionalities that can be tailored for different requirements. The size of the NCs affects the uptake efficiency through the different cell lines and kinetics to reach the targeted organ or tissue cells.[23,24] The optimal NCs size should be below 50 nm for active uptake into live cells.

Recently, perovskite NCs have been used as fluorophores for the detection of different metal ions, owing to their excellent emission properties.[25–31] There are reports of Cu^{2+}-ion detection in the presence of highly stable lower-dimensional perovskite NCs in aqueous media.[32–34] $CsPbX_3$ NCs have been proven to be a potential fluorescent probe for Cu^{2+}-ion detection in organic, bio, and industrial oils.[29–31,35] Most of these experiments were performed in nonpolar solvents to avoid the degradation of perovskite NCs due to their poor structural stability.[36,37] These non-polar solvents are immiscible in aqueous media, which restricts metal ion detection in the biological systems or natural resources. So, highly water stable and water dispersible fluorescent

Department of Engineering and Materials Physics, Institute of Chemical Technology-IndianOil Odisha Campus, Mouza-Samantapuri, Bhubaneswar, Odisha, 751013, India. E-mail: s.bhaumik@iocb.ictmumbai.edu.in

† Electronic supplementary information (ESI) available. See DOI: https://doi.org/10.1039/d2ma00719c

probes are required such that the detection efficiency of metal ions can be improved. The perovskite NCs are usually encapsulated with oleic acid (OAc) and oleylamine (OAm) ligands, which are very dynamic and unstable. So, the NCs are very prone to degradation in the presence of heat, water, or intense UV light. It's a basic need to improve the perovskite structural stability for implementing them in real-world activities. Shelling of perovskite NCs with different stable materials is an effective way to further improve the NCs' stability and luminous intensity. These shelling materials protect the core from external harsh environments and maintain high emission intensity and stability for a longer time period. Bhaumik *et al.* synthesized methylammonium lead bromide ($MAPbBr_3$) core and layered octylammonium lead bromide [$(OA)_2PbBr_4$] shell NCs by a ligand-assisted reprecipitation (LARP) synthetic method, demonstrating better structural stability and luminescence intensity that persisted for several months.[38]

In succession, various research groups reported the coating of perovskite NCs with various stable shelling materials, such as lower-dimensional perovskites, metal oxide layers, metal sulfide layers, or bulky polymers.[39–49] $CsPbX_3$@Cs_4PbX_6 and $CsPbBr_3$@Rb_4PbBr_6 core@shell NCs were also synthesized *via* a hot-injection method that shows higher luminescence intensity and superior photostability.[50–52] The polymers are usually flexible and increase the hydrophobicity of NCs, which improves the water stability. Polyvinyl-pyrrolidone (PVP) polymer encapsulated $CsPbBr_3$ NCs embedded in a polystyrene (PS) matrix exhibited better water resistance and were demonstrated as luminescent probes in live cells.[53] PVP-coated $CsPbBr_3$ NCs surrounded by a polymethyl methacrylate (PMMA) matrix were also explored for live-cell imaging.[54] *N*-isopropyl acrylamide (NIPAM) was also extensively exploited as a thermosensitive polymer for biomedical applications and drug delivery.[55–57] Silica-coated perovskite NCs are mostly explored due to their better stability in water.[48,58] This synthesis procedure required a longer reaction time for the completion of the hydrolysis and condensation processes of silane groups for the growth of a thick silica shell around the NCs. The silica-coated NCs also tend to agglomerate among themselves and become bigger particles for reduction of surface energy, resulting in non-uniform particle size distributions.[42,59] These agglomerations among NCs also lead to an increase in NCs reabsorption and scattering, causing a decrease in the NCs luminous intensity and device efficiency.

Here in this work, we tried to find an easy and robust synthesis protocol that can be suitable for industrial processing. We report the synthesis of $CsPbBr_3$ NCs *via* a one-pot LARP synthetic approach under normal atmospheric conditions (relative humidity level above 80%). Here, we encapsulated the $CsPbBr_3$ NCs with different stable materials, such as SiO_2, PVP, or mixed PVP-NIPAM polymers, and then investigated their structural and emission properties. In the case of silica-coated NCs, we selected (3-aminopropyl)trimethoxysilane (APTMS) as a silica source because APTMS binds the $CsPbBr_3$ NCs surface with their amino groups while the alkoxysilane groups hydrolyze to form silanol groups in the presence of a trace amount of water in toluene solvent during the synthesis process.[48,60] Furthermore, silanol groups condensate to form silica coatings around the NCs. In the case of the polymer coating, PVP and NIPAM polymers were used as shelling materials that attach to the NC surface and help to control the NCs growth. PVP gets adsorbed to the surface of the NCs, and further, NIPAM and PVP intertwine among themselves to form a protective shell that protects the NCs core from the harsh atmosphere. OAc and OAm ligands are also added during the NCs synthesis process such that OAc ligands prevent agglomeration among the perovskite NCs, while the amino groups of the OAm ligands attach to the NCs surface and improve NCs solution stability.[61] Finally, we used the most stable polymer-coated NCs as a luminescence agent to investigate their Cu^{2+}-ion detection ability in water. Since the degradation of perovskite NCs becomes slower in water for effective polymer coating, this permits the detection of Cu^{2+}-ions directly in water with high sensitivity. This work paves a way to detect Cu^{2+}-ions in biological systems or natural resources.

Experimental section

Materials

Cesium bromide (CsBr, 99.999% trace metals basis); lead(II) bromide ($PbBr_2$, 99.999% trace metals basis); *n*-dimethylformamide (DMF, anhydrous, 99.8%); (3-aminopropyl)trimethoxysilane (APTMS, 97%); oleic acid (OAc, 90%); oleylamine (OAm, 70%); poly(vinyl pyrrolidone) (PVP, avg. M_n 6000, PDI $\leq$ 1.2); *n*-isopropylacrylamide (NIPAM, 97%); acetonitrile (ACN, 99.95%); toluene (anhydrous, 99.8%); zinc bromide ($ZnBr_2$, 99.9%, trace metal basis); and ethanol (anhydrous, 99.8%) were purchased from Sigma Aldrich company. *n*-Octylammonium bromide (OABr, 99%) was purchased from Greatcell solar materials company. Nickel(II) chloride hexahydrate (98%) was purchased from Sisco research laboratories private limited. Aluminium chloride hydrated (97%, AR Grade) was purchased from SD Fine Chem limited. Indium(III) acetate (99.99%) was purchased from Alfa Aeser company. Cobalt nitrate (97%) was purchased from Nice chemicals private limited. Iron(II) chloride hydrate (95%) was purchased from Central drug house private limited. Iron(III) chloride (anhydrous, 98%) was purchased from Avra synthesis private limited. Cupric acetate (98%) was purchased from Qualigens company. All chemicals were used without further purification.

Synthesis of SiO_2-coated $CsPbBr_3$ NCs

Silica-coated $CsPbBr_3$ NCs were synthesized *via* a modified ligand assisted re-precipitation (LARP) method.[48] First, three separate precursor solutions were prepared by dissolving 0.02 mmol (4.2 mg) CsBr in 250 μL of DMF, 0.02 mmol (4.2 mg) OABr in 250 μL of DMF, and 0.02 mmol (7.34 mg) $PbBr_2$ in 250 μL of DMF and mixed properly *via* stirring to complete dissolution. Next 200 μL of CsBr precursor and 50 μL of OABr precursor (CsBr : OABr = 8 : 2) were injected into the $PbBr_2$ precursor solution and mixed properly. Finally, 10 μL of APTMS was injected into the $PbBr_2$ precursor to form the final precursor. 250 μL of the final precursor was quickly injected

dropwise in a round bottom flask containing 5 mL of toluene under vigorous stirring conditions. The stirring was continued for 4 hours to complete the hydrolysis process of APTMS. The NC solution was then centrifuged at 3000 rpm for 15 min. The supernatant was discarded and the precipitate was dispersed in 1 mL of ethanol for further characterization. The NCs are renamed CPB-SiO_2 for better understanding.

Synthesis of PVP and mixed PVP-NIPAM coated $CsPbBr_3$ NCs

PVP-coated $CsPbBr_3$ NCs were synthesized *via* a modified LARP method.[48] At first, three separate precursor solutions were prepared by dissolving 0.02 mmol CsBr in 250 μL DMF, 0.02 mmol OABr in 250 μL DMF, and 0.02 mmol $PbBr_2$ in 250 μL DMF under vigorous stirring conditions. Next, 200 μL of CsBr precursor and 50 μL of OABr precursor (CsBr : OABr = 8 : 2) were injected into the $PbBr_2$ precursor solution and mixed properly. Finally, 50 μL of OAc and 25 μL of OAm were added to the mixture solution to form the final precursor. 250 μL of the final precursor was injected dropwise into a round bottom flask containing 5 mL toluene and 4 mg PVP under vigorous stirring. The reaction was continued for 30 min and then the reaction was stopped. The resulting $CsPbBr_3$ NC solution (renamed PbN-1) was transferred to a centrifuge tube and then 2 mL ACN was added. The mixture was centrifuged at 6000 rpm of speed for 15 min and the precipitate was dispersed in 1 mL toluene or water for further characterization. The mixed PVP-NIPAM coated $CsPbBr_3$ NCs were synthesized following the same method with slight modification in which the amount of PVP (~4 mg) was kept fixed while variable amounts of NIPAM (5 mg: PbN-2, 10 mg: PbN-3, 15 mg: PbN-4, and 20 mg: PbN-5) were added.

Results and discussion

Schematic diagrams of the encapsulation process of $CsPbBr_3$ NCs with silica, and coating with PVP and NIPAM polymers during the synthesis process are shown in Fig. S1a and b (in the ESI†). The silica and PVP-coated $CsPbBr_3$ NCs are represented as CPB-SiO_2 and PbN-1 NCs, respectively. While the samples with a successive increase in NIPAM polymer in the PbN-1 NCs are denoted as PbN-2, PbN-3, PbN-4, and PbN-5 NCs, respectively.

The X-ray diffraction (XRD) pattern of CPB@SiO_2 and different PbN NCs in thin-film form are demonstrated in Fig. 1. The diffraction pattern for the CPB@SiO_2 NCs thin-film reveals mixed perovskite phases, *i.e.*, 3D $CsPbBr_3$ (monoclinic phase) and 0D Cs_4PbBr_6 (rhombohedral phase) crystal structures. Similar mixed-phase perovskite NCs were already reported when the silica-coated $CsPbBr_3$ NCs were synthesized *via* the LARP synthesis method.[10,62] Significant XRD diffraction peaks are observed at 2θ values of 15.45°, 21.76°, 30.56°, 34.7°, 37.94°, and 44.38° that correspond to the (100), (110), (002), (201), (211), and (202) lattice planes of the 3D monoclinic $CsPbBr_3$ crystal structure (PDF #00-18-0364).[10,62] The additional XRD diffraction peaks located at 2θ values of 12.91°, 20.34°, 22.66°, 25.68°, 27.77°,

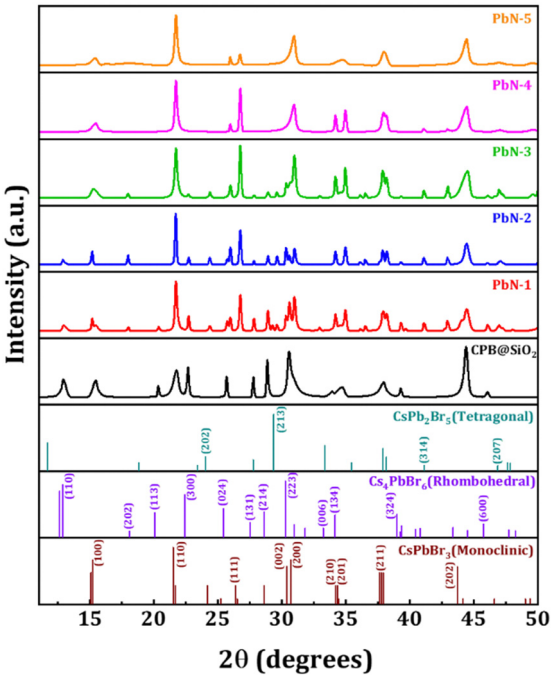

Fig. 1 Stacked XRD diffraction patterns of different NCs in thin-film form. The bottom of the figure represents the standard XRD diffraction patterns of monoclinic $CsPbBr_3$, rhombohedral Cs_4PbBr_6, and tetragonal $CsPb_2Br_5$ perovskite structures.

28.84°, 30.55°, 34.18°, 39.26°, and 46.07° signify the (110), (113), (300), (024), (131), (214), (223), (134), (324), and (600) lattice planes of the rhombohedral Cs_4PbBr_6 crystal structure (PDF #01-73-2478).[50,63] The contribution of rhombohedral Cs_4PbBr_6 phases is quite high as compared to monoclinic $CsPbBr_3$ phases. The XRD diffraction pattern of PbN-1 NCs reveals three perovskite phases, *i.e.*, 3D $CsPbBr_3$ (monoclinic phase), 0D Cs_4PbBr_6 (rhombohedral phase), and 2D $CsPb_2Br_5$ (tetragonal phase) crystal structures. The XRD diffraction peaks obtained at 2θ values of 15.18°, 26.75°, 30.96°, and 34.17° signify the (001), (111), (200), and (210) lattice planes of the monoclinic $CsPbBr_3$ crystal structure. Two additional XRD peaks observed at 18.01° and 30.97° correspond to the (202) and (006) lattice planes of the rhombohedral Cs_4PbBr_6 crystal structure. Some additional XRD peaks obtained at 2θ values of 24.36°, 29.25°, 41.08°, and 46.96° correspond to (202), (213), (314), and (207) lattice planes of the tetragonal $CsPb_2Br_5$ crystal structure (PDF#25-0211).[45,64] With an increase in NIPAM amount (*i.e.*, PbN-2, PbN-3, PbN-4, and PbN-5 NCs) in the PbN-1 NCs, there is a minimal change in the monoclinic $CsPbBr_3$ crystal phases. In contrast, an abrupt reduction in rhombohedral Cs_4PbBr_6 and tetragonal $CsPb_2Br_5$ crystal phases is noticed. The XRD diffraction peaks related to $(OA)_2PbBr_4$ perovskite phases can't be detected due to the formation of a very thin shell layer and below the XRD instrument detection limit.[38,48]

The shape and size of the NCs are investigated using transmission electron microscopy (TEM) and high-resolution transmission electron microscopy (HRTEM) imaging. The TEM and HRTEM images of CPB@SiO_2 and PbN NCs are shown in

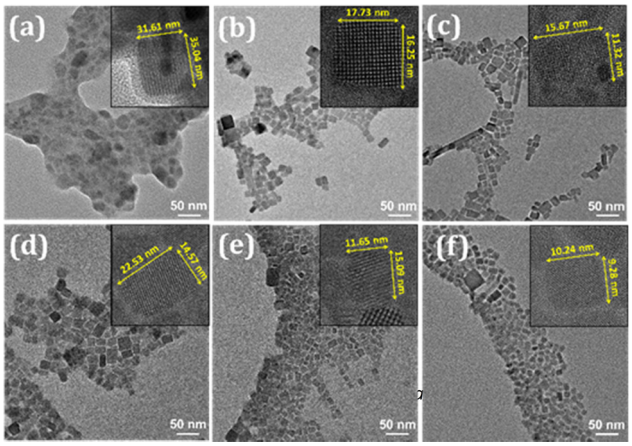

Fig. 2 TEM and HRTEM (inset) images of (a) CPB@SiO_2, (b) PbN-1, (c) PbN-2, (d) PbN-3, (e) PbN-4, and (f) PbN-5 NCs.

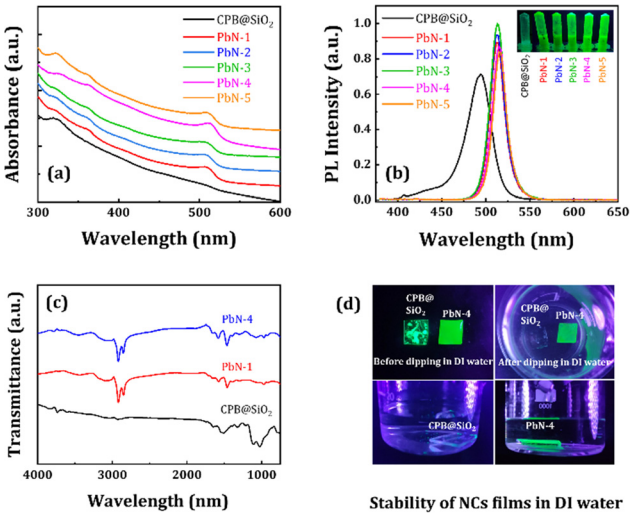

Fig. 3 (a) Absorption and (b) PL spectra of CPB@SiO_2 and PbN NCs as marked in the legend. The inset of (b) represents the photographic image of all NCs in the solution phase under a UV lamp. (c) FTIR spectra of CPB@SiO_2, PbN-1, and PbN-4 NCs. (d) Photographic images of CPB@SiO_2 and PbN-4 NCs thin-films after being dipped in DI water and placed under a UV lamp.

Fig. 2, and the corresponding particle size distributions are represented shown in Fig. S2 (in ESI†). The slightly blurry surfaces around the CPB@SiO_2 NCs (see Fig. 2a) appeared from the adsorption of the silica coating that is compact and has a shell thickness of a few nm. The silica shells diffuse among other silica-coated NCs and transform into bigger irregular shapes. The average particle size distribution of the CPB@SiO_2 NCs is 32 ± 7 nm, which is quite big in size. These NCs exhibit inter-planar spacing of 0.42 nm that corresponds to the (110) lattice planes of monoclinic $CsPbBr_3$ crystal phases.[65] In comparison, the polymer-coated PbN NCs (see Fig. 2b–f) reveal a monodisperse and uniform particle size distribution without any noticeable inter-particle agglomeration. These PbN NCs are cubic in shape and highly crystalline in nature. A similar (110) lattice plane appeared for the PbN NCs from the monoclinic $CsPbBr_3$ crystal structures. The mean particle sizes of PbN-1, PbN-2, PbN-3, PbN-4, and PbN-5 NCs are around 13.47 ± 3, 13.2 ± 3, 13.1 ± 3, 10.7 ± 2, and 10.2 ± 2 nm, respectively (see Fig. S2 in the ESI†). It can be seen that the particle size becomes smaller and the particle size distribution is more uniform with an increase in the amount of NIPAM polymer. It is beneficial for strong quantum confinement of charge carriers inside the NCs and hence enhances the optical properties.

The UV-vis absorption spectra of all the NCs in the solution phase are shown in Fig. 3a. The absorption spectrum of CPB@SiO_2 reveals a band edge peak at 507 nm originated due to 3D $CsPbBr_3$ perovskites and a minor peak at 320 nm that appeared from 0D Cs_4PbBr_6 perovskites.[11] The PbN NCs demonstrate nearly similar absorption spectra while more intense, sharper, and well-defined absorption band edges are observed. The scattering effect of CPB@SiO_2 NCs is much higher as compared to PbN NCs because of the bigger particle sizes of CPB@SiO_2 NCs.[66,67] The band edge absorption peaks of PbN NCs are slightly redshifted with increasing the NIPAM polymer. The PL emission spectra of CPB@SiO_2 NCs (dispersed in ethanol) and PbN NCs (dispersed in toluene) are shown in Fig. 3b. The corresponding photographic images of all NCs under a UV lamp are shown in the inset of Fig. 3b. The CPB@SiO_2 NCs emit a cyan-green color emission with a PL peak position at 494 nm. These NCs showed emission PLQY up to 63% with an FWHM of 31 nm. The low emission intensity of the CPB@SiO_2 NCs is resulted due to the presence of unwanted Cs_4PbBr_6 phases that don't contribute to the radiative recombination. The polymer-coated PbN NCs are more luminescent compared to silica-coated NCs due to the reduction of the Cs_4PbBr_6 phases. The PbN NCs also reveal narrower emission spectra and better emission intensity, denoting efficient radiative recombination and higher color purity. The emission peak for PbN-1 NCs is obtained at 513 nm with a very narrow FWHM of 21 nm. Initially, with the addition of NIPAM polymer up to a certain limit, the emission intensity of the PbN NCs was increased. The further increment of NIPAM polymer resulted in a reduction of the NCs PL intensity. The binding constant of the NIPAM was estimated from the change in the emission intensity of the PbN NCs with an increase in NIPAM concentration.[68] The binding constant was calculated from the intercept of the plot and it comes close to 8787 M^{-1} (see Fig. S4, ESI†). Among all these PbN NCs, the PbN-3 NCs demonstrate the highest emission intensity with a maximum PLQY up to 93%. The CIE color coordinates of the CPB@SiO_2 and PbN-3 NCs are calculated as (0.071, 0.395) and (0.079, 0.723), respectively (see Fig. S3 in the ESI†). The subsequent information regarding the PL peak position, FWHM, and PLQYs of all NCs is tabulated in Table 1.

We performed Fourier transform infrared spectroscopy (FTIR) analysis for all NCs, and the subsequent plots are represented in Fig. 3c. The spectrum for CPB@SiO_2 NCs reveals strong absorption peaks located at 1107 and 754 cm^{-1} due to antisymmetric stretching of Si–O–Si bonds and symmetrical stretching of Si–O bonds, respectively.[59,60] The additional peaks at 2927 and 2874 cm^{-1} appeared due to asymmetric and symmetric stretching of C–H bonds, respectively. The enrichment of

Table 1 Optical properties of different coated NCs

Name of the NCs	PL peak position (nm)	FWHM (nm)	PLQY (%)
CPB@SiO_2	494	31	63
PbN-1	513	21	83
PbN-2	513	21	87
PbN-3	513	22	93
PbN-4	515	21	81
PbN-5	515	20	78

the Si–O–Si and Si–O vibration peaks confirms the silica coating around the NCs after the hydrolysis process. The FTIR spectra for the PbN NCs reveal strong absorption peaks at 1294, 1650, and 3500 cm^{-1} corresponding to C–N, C═O, and N–H bonding vibrations of the PVP and NIPAM polymers, respectively.[53–56] These vibration peaks confirm the presence of a polymer coating around the PbN NCs. There is also an absorption peak at 3100 cm^{-1} corresponding to –OH stretching vibrations from the presence of OAc. Additionally, the absorption peak intensities at 1650–1660 and 3500 cm^{-1} became intense with an increase in NIPAM polymer (PbN-4 NCs) compared to without NIPAM (PbN-1 NCs), revealing stronger C═O bonding interactions and N–H bonding vibrations, respectively. There was also a decrease in peak intensity at 3100 cm^{-1} with an increase in NIPAM polymer in the PbN-1 NCs, revealing the weakening of the –OH bonds.

The PbN NCs can easily be dispersed in water and maintained their luminescence properties for several days. The photographic image of the water dispersed PbN NCs under a UV lamp is shown in Fig. S5 (in the ESI†). We examined the water stability of the CPB@SiO_2 and PbN-4 NCs in thin-film form by dipping them into a glass beaker containing DI water. The photographic images of the thin-films under a UV lamp are shown in Fig. 3d. The silica-coated NCs tend to agglomerate among themselves on the glass substrate and result in non-uniform film morphology. After dipping the CPB@SiO_2 NCs thin-film into DI water, the luminescence of the NCs quenched instantly. In comparison, the coverage of the PbN-4 NCs thin-film is relatively better, and a smooth surface was formed due to lower surface energy after polymer coating, which is a prerequisite for the fabrication of efficient thin-film based LEDs.[69,70] The emission intensity of the PbN-4 NCs thin-film was retained for a longer time period, demonstrating ultra-high stability of the PbN NCs films in water. These results conclude that the coating of PVP and NIPAM polymers around the NCs significantly improves the NCs emission intensity and crystal structural stability.

Furthermore, we performed a water stability test of all NCs in the solution phase. At first, we prepared a 5 mg mL^{-1} concentrated CPB@SiO_2 NCs solution dispersed in ethanol, and the same concentration PbN NCs solution dispersed in water (since toluene and water are immiscible). We started with 100 μL of each NCs solution in separate glass vials followed by the addition of 50 μL of DI water in sequence. We measured the amount of DI water required to completely degrade the perovskite structures, *i.e.*, when the luminescence from the NCs was mostly quenched (PL intensity nearly zero). The PL spectra of the CPB@SiO_2, PbN-1, and PbN-4 NCs for the water-stability test are shown in Fig. 4a–c and the remaining NCs are represented in Fig. S6 (in ESI†). The CPB@SiO_2 NCs degrade much faster, in which the emission color started shifting from green to blue color with addition of just 50 μL DI water (PL quenched by 73%) and the total emission was quenched in the presence of 250 μL DI water (around 96% of PL quenching). The blue emission spectrum is originated from transformation of 3D perovskite structures to comparatively stable lower dimensional perovskite structures.[71,72] The water stability of the polymer coated PbN NCs is significantly improved with increasing the NIPAM polymer and hardly any emission shift is noticed. Fig. 4d shows the change in PL intensity for all NCs with the addition of DI water. The PL retention percentages for CPB@SiO_2, PbN-1, PbN-2, PbN-3, PbN-4, and PbN-5 NCs are 4%, 23%, 31%, 50%, 57%, and 53%, respectively, with addition of 250 μL DI water in the corresponding NCs solutions. The PbN-4 NCs exhibit the best water stability. The emission intensity of the PbN-4 NCs remains 21% of the original PL intensity even after the addition of 1000 μL DI water. The photographic images of all the NCs solutions after the addition of DI water are shown in Fig. S7 (in the ESI†).

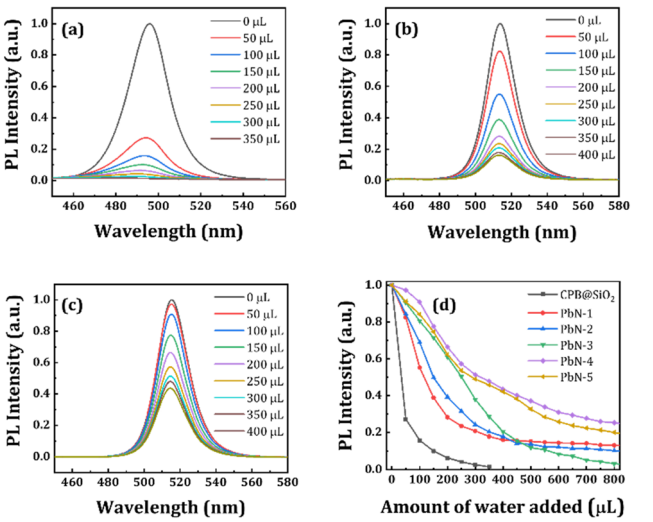

Fig. 4 PL spectra of (a) CPB@SiO_2, (b) PbN-1, and (c) PbN-4 NCs solutions with different amounts of DI water added to the corresponding NCs solution, as shown in the legends. (d) The change in PL intensity of all NCs with the addition of water, as shown in the legend.

We also performed a water stability test for all NCs in powder form as a function of time. Here, 100 μL of DI water was added to the same amount of NC powders and kept under a UV lamp. Then we recorded the changes in emission spectra at regular time intervals in a PL spectrometer. The corresponding emission spectra of the CPB@SiO_2, PbN-1, and PbN-4 NCs are represented in Fig. 5a–c and the emission spectra of the remaining samples are shown in Fig. S8 (in ESI†). Among them, the SiO_2-coated NCs are least stable under direct water contact and degraded within 10 min. Fig. 5d represents the change in emission spectra of all NCs with different time intervals after the addition of DI water. However, the polymer-coated NCs maintained their emission intensity in water for longer periods

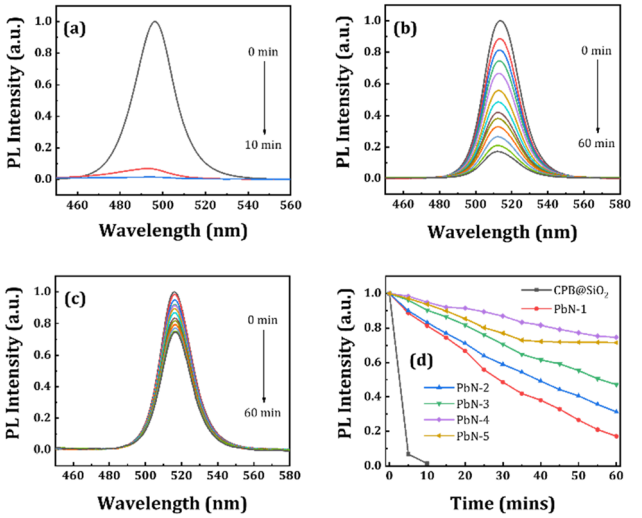

Fig. 5 PL spectra of (a) CPB@SiO_2, (b) PbN-1, and (c) PbN-4 NCs at a time interval of 5 min after the addition of 100 μL DI water in 100 μL of NCs solution. (d) The change in PL intensity of all NCs samples after 100 μL DI water addition as a function of time, as shown in legend.

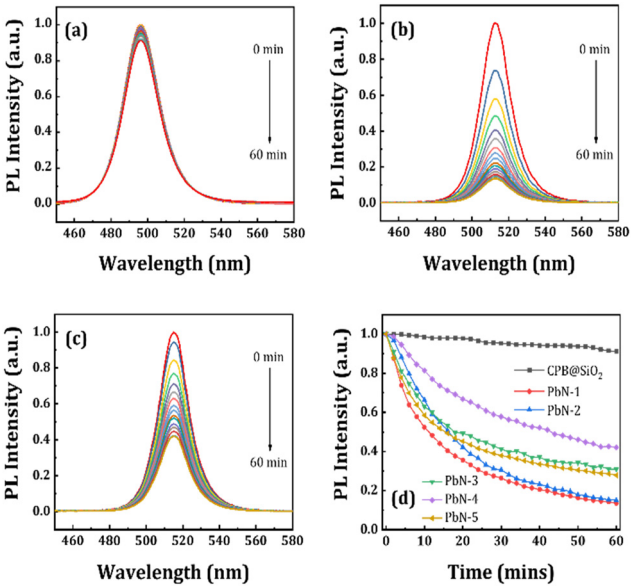

Fig. 6 Heat stability test: PL spectra of (a) CPB@SiO_2, (b) PbN-1, and (c) PbN-4 NCs films for a period of 60 min while kept under 60 °C. (d) The changes in PL intensity of all NCs samples kept at 60 °C as a function of time, as shown in legend.

of time. The PL intensity of the CPB@SiO_2 NCs degrades almost 99% of its initial PL intensity within 10 min. While the PbN-1, PbN-2, PbN-3, PbN-4, and PbN-5 NCs retained 81%, 83%, 90%, 94%, and 93%, respectively, of their initial PL intensity within the same time period. After 60 min, the PL intensity retention percentages of the PbN-1, PbN-2, PbN-3, PbN-4, and PbN-5 NCs are recorded as 17%, 31%, 47%, 74%, and 71%, respectively. These observations conclude that the PbN-4 NCs show the best water stability. The photographic images of all NCs after the addition of DI water with regular time intervals under a UV lamp are shown in Fig. S9 (see ESI†).

We also performed a heat stability test of all NCs in thin-film form. The glass substrates were coated with different NCs to form separate thin-films and placed on a hot-plate (temperature ∼ 60 °C). The PL intensities of the NCs thin-films were recorded by a PL spectrometer as a function of time. The PL spectra of the CPB@SiO_2, PbN-1, and PbN-4 NCs thin-films with different time intervals under heating conditions are shown in Fig. 6a–c, and the PL spectra of the remaining NCs are represented in Fig. S10 (see ESI†). We observed that the heat stability of the CPB@SiO_2 NCs is the highest among all NCs. The retention in PL intensity is 95% after 32 min and 91% after 60 min of time. The high thermal stability of the SiO_2-coated NCs is due to the lower thermal conductivity of silica.[73,74] The silica shell acts as a thermal insulation layer that protects the core material against degradation in the presence of heat. Fig. 6d shows the curve representing the change in PL intensity with time. Among the polymer-coated NCs, the PbN-4 NCs also had the highest heat stability. After 32 min of time, the PL retentions for the PbN-1, PbN-2, PbN-3, PbN-4, and PbN-5 NCs are 26%, 30%, 41%, 57%, and 37%, respectively. Similarly, after 60 min the PL retentions for the PbN-1, PbN-2, PbN-3, PbN-4, and PbN-5 NCs are 13%, 15%, 30%, 42%, and 27%, respectively. These results indicate that the heat stability of the NCs increases with a certain increase in the amount of NIPAM polymer.

The instability of the perovskite NCs in water limits the detection of metal ions in an aqueous atmosphere.[36,37] The comparatively higher water stability of the PbN-4 NCs encouraged us to further investigate their capability to detect metal ions in water media. To perform the ion detection experiment, we prepared different aqueous solutions containing Ni^{2+}, Al^{3+}, In^{3+}, Co^{2+}, Fe^{2+}, Fe^{3+}, and Cu^{2+}-ions. Then these solutions were added separately in the same concentrated PbN-4 NCs solution (∼5 mg mL^{-1}) dispersed in DI water. The subsequent photographic images of the NCs solutions before and after the addition of different metal ion solutions are shown in Fig. 7a. The emission of the PbN-4 NCs solution is totally quenched with the addition of Cu^{2+}-ion solution while the PL intensity of other NCs solutions remained almost unchanged (see Fig. 7b). The PL quenching of the NC solution in the presence of Cu^{2+}-ions determines the detection capability of Cu^{2+}-ions in the aqueous solution. Furthermore, we recorded the emission spectra of the PbN-4 NCs solution in the presence of different concentrations of Cu^{2+}-ions varied from 0 to 412 μM. With the increase of the concentration of Cu^{2+}-ions, the PL intensity of the PbN-4 NCs is monotonically decreased (see Fig. 7c and d) while the shape of the PL spectra remained unchanged or not shifted. The linear decrease in PL intensity with an increase in Cu^{2+}-ions confirms the high detection capabilities towards Cu^{2+}-ions in the presence of PbN-4 NCs, and the probing window is quite wide. The possible reason for quenching of PL could be due to the transfer of electrons from NCs to Cu-ions,[31] or adsorption of Cu^{2+}-ions to the NC surface.[31] Several fluorescence quenching mechanisms have been explained to describe the energy or charge transfer between donor and

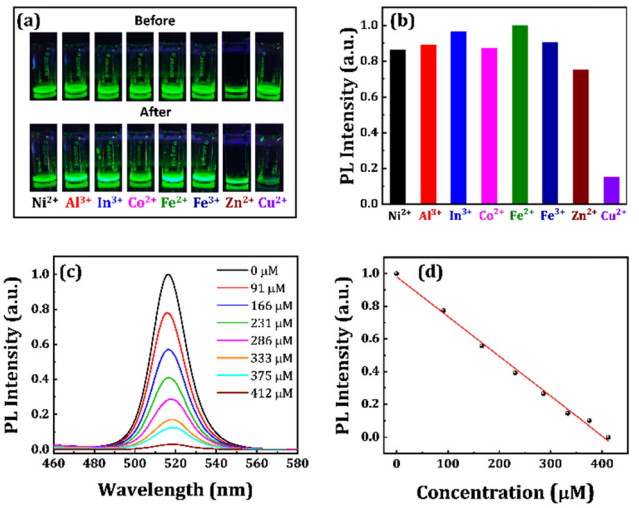

Fig. 7 Photographic images of the PbN-4 NCs solution under a UV lamp (a) before and after the addition of different metal ions as marked in the figure. (b) Chart representing the comparison of the PL intensity of PbN-4 NCs that persisted after the addition of subsequent metal ions. (c) Emission spectra of PbN-4 NCs in the presence of different concentrations of Cu^{2+}-ion solutions as shown in the legends. (d) Linear curve representing a decrease in PL intensity of PbN-4 NCs after the addition of different concentrations of Cu^{2+}-ion solution.

acceptor materials, such as fluorescence resonance energy transfer (FRET), cation exchange, and electron transfer processes.[75–77] There is no spectral shift observed in the case of PbN-4 NCs after the addition of Cu^{2+}-ions (see Fig. 7c). In the cation exchange process, the emission peak usually shifts either to higher/lower energies.[77] So, the possibility of the cation exchange with Cu^{2+}-ions in PbN-4 NCs is not feasible. The absorption spectra of the acceptors and emission spectra of the donors should overlap for the FRET mechanism.[78] However, no such overlap is noticed between the emission spectrum of the PbN-4 NCs and absorption spectrum of copper acetate (see Fig. S11, ESI†). Generally, the electron transfer process exhibits linear emission quenching with the increase of metal-ion concentration.[31] Similar emission quenching behaviour is observed in our system. This is attributed to the special d^9 electronic configuration of Cu^{2+}-ions, which is favourable to accept an electron and shift to a comparatively stable d^{10} electronic configuration.[79,80] A schematic diagram of the charge transfer process in the presence of Cu^{2+}-ions is shown in Fig. S12 (see ESI†). If the Cu^{2+}-ions come into close proximity to PbN-4 NCs, they are adsorbed on the NC surface, triggering the charge transfer from the NCs to the Cu^{2+}-ions. Consequently, the radiative transition from the conduction band to the valence band of the NCs is inhibited and results in PL quenching of the NCs. In order to find the detection limit of Cu^{2+}-ions, we plotted the first four lowest concentrations at which the PL intensity of the NCs solution starts quenching and linear-fitted the points. To find the detection limit, we used the (3σ/slope) formula.[81,82] The slope and σ (standard deviation) are calculated from the linear fit. Using the above formula, the lowest detection limit for the detection of Cu^{2+}-ions is found to be 18.6 μM (R^2 = 0.9986) based on the slope (=0.00266) and σ (=0.01658) values. These results are extremely beneficial for Cu^{2+}-ion detection in natural water resources and biological systems.

Conclusions

In conclusion, we report the synthesis of $CsPbBr_3$ NCs *via* a one-pot modified LARP synthetic approach under normal atmospheric conditions (relative humidity level above 80%) where the NCs were coated with different materials, such as SiO_2, PVP, and mixed PVP-NIPAM polymers. The silica-coated NCs are made of $CsPbBr_3$-Cs_4PbBr_6 nanocomposites, while the polymer-coated NCs consist of a trace amount of 2D $CsPb_2Br_5$ perovskite phase along with $CsPbBr_3$-Cs_4PbBr_6 nanocomposites. The SiO_2-coated NCs exhibit PL peak position at 494 nm (FWHM ~ 31 nm) with a maximum PLQY up to 63%. These NCs are quite big and the particle size distribution is also broad. With PVP and NIPAM polymer coating around the NCs, the PL intensity and water stability of the NCs significantly improved, but the heat stability decreased compared to SiO_2-coated NCs. The polymer-coated NCs can be dispersible in water and maintain their PL intensity for many days. These NCs exhibit a definite shape and size with narrow size distribution that is suitable for the intake of NCs in biological cells. These NCs emit green emission in the spectral range of 513–515 nm with a maximum PLQY up to 93%. The emission FWHM of the NCs is also decreased which is beneficial for display technologies. The polymer-coated NCs exhibited better water stability as compared to the mostly used SiO_2-coated NCs, enabling them to perform Cu^{2+}-ion detection directly in an aqueous solution. These results are extremely valuable and can be used for the detection of Cu^{2+}-ions in natural water resources and biological systems.

Author contributions

S. B. conceived the research idea and planned the experiments accordingly. M. R. K. performed the synthesis, characterization, and related experiments. U. P. assisted M. R. K. during the experiments. The manuscript was written through contributions from all authors. All authors have given approval to the final version of the manuscript.

Conflicts of interest

There are no conflicts to declare.

Acknowledgements

S. B. acknowledges the Department of Science and Technology (DST), India (Award number# DST/INSPIRE/04/2017/000530) and the Science and Engineering Research Board (SERB), India (Award number# SRG/2019/000093) for financial support. We also acknowledge the ICT-IOC start-up research grant for financial support.

Notes and references

1 M. V. Kovalenko, L. Protesescu and M. I. Bodnarchuk, Properties and potential optoelectronic applications of lead halide perovskite nanocrystals, *Science*, 2017, **358**, 745–750.
2 Q. A. Akkerman, G. Rainò, M. V. Kovalenko and L. Manna, Genesis, challenges and opportunities for colloidal lead halide perovskite nanocrystals, *Nat. Mater.*, 2018, **17**, 394–405.
3 A. Swarnkar, A. R. Marshall, E. M. Sanehira, B. D. Chernomordik, D. T. Moore, J. A. Christians, T. Chakrabarti and J. M. Luther, Quantum dot–induced phase stabilization of α-CsPbI3 perovskite for high-efficiency photovoltaics, *Science*, 2016, **354**, 92–95.
4 Y. Zhao and K. Zhu, Organic–inorganic hybrid lead halide perovskites for optoelectronic and electronic applications, *Chem. Soc. Rev.*, 2016, **45**, 655–689.
5 X.-K. Liu, W. Xu, S. Bai, Y. Jin, J. Wang, R. H. Friend and F. Gao, Metal halide perovskites for light-emitting diodes, *Nat. Mater.*, 2021, **20**, 10–21.
6 Y.-H. Kim, S. Kim, A. Kakekhani, J. Park, J. Park, Y.-H. Lee, H. Xu, S. Nagane, R. B. Wexler, D.-H. Kim, S. H. Jo, L. Martínez-Sarti, P. Tan, A. Sadhanala, G.-S. Park, Y.-W. Kim, B. Hu, H. J. Bolink, S. Yoo, R. H. Friend, A. M. Rappe and T.-W. Lee, Comprehensive defect suppression in perovskite nanocrystals for high-efficiency light-emitting diodes, *Nat. Photonics*, 2021, **15**, 148–155.
7 D. Liu, Y. Guo, M. Que, X. Yin, J. Liu, H. Xie, C. Zhang and W. Que, Metal halide perovskite nanocrystals: application in high-performance photodetectors, *Mater. Adv.*, 2021, **2**, 856–879.
8 W. Chen, S. Bhaumik, S. A. Veldhuis, G. Xing, Q. Xu, M. Grätzel, S. Mhaisalkar, N. Mathews and T. C. Sum, Giant five-photon absorption from multidimensional core-shell halide perovskite colloidal nanocrystals, *Nat. Commun.*, 2017, **8**, 15198.
9 L. Protesescu, S. Yakunin, M. I. Bodnarchuk, F. Krieg, R. Caputo, C. H. Hendon, R. X. Yang, A. Walsh and M. V. Kovalenko, Nanocrystals of Cesium Lead Halide Perovskites (CsPbX3, X = Cl, Br, and I): Novel Optoelectronic Materials Showing Bright Emission with Wide Color Gamut, *Nano Lett.*, 2015, **15**, 3692–3696.
10 L. Xu, J. Li, T. Fang, Y. Zhao, S. Yuan, Y. Dong and J. Song, Synthesis of stable and phase-adjustable CsPbBr3@Cs4PbBr6 nanocrystals via novel anion–cation reactions, *Nanoscale Adv.*, 2019, **1**, 980–988.
11 S. Bhaumik, S. A. Veldhuis, S. K. Muduli, M. Li, R. Begum, T. C. Sum, S. Mhaisalkar and N. Mathews, Inducing Isotropic Growth in Multidimensional Cesium Lead Halide Perovskite Nanocrystals, *ChemPlusChem*, 2018, **83**, 514–520.
12 B.-S. Zhu, H.-Z. Li, J. Ge, H.-D. Li, Y.-C. Yin, K.-H. Wang, C. Chen, J.-S. Yao, Q. Zhang and H.-B. Yao, Room temperature precipitated dual phase CsPbBr3–CsPb2Br5 nanocrystals for stable perovskite light emitting diodes, *Nanoscale*, 2018, **10**, 19262–19271.
13 J. Shamsi, A. S. Urban, M. Imran, L. De Trizio and L. Manna, Metal Halide Perovskite Nanocrystals: Synthesis, Post-Synthesis Modifications, and Their Optical Properties, *Chem. Rev.*, 2019, **119**, 3296–3348.
14 A. Dutta, R. K. Behera, P. Pal, S. Baitalik and N. Pradhan, Near-Unity Photoluminescence Quantum Efficiency for All CsPbX3 (X = Cl, Br, and I) Perovskite Nanocrystals: A Generic Synthesis Approach, *Angew. Chem., Int. Ed.*, 2019, **58**, 5552–5556.
15 G. Nedelcu, L. Protesescu, S. Yakunin, M. I. Bodnarchuk, M. J. Grotevent and M. V. Kovalenko, Fast Anion-Exchange in Highly Luminescent Nanocrystals of Cesium Lead Halide Perovskites (CsPbX3, X = Cl, Br, I), *Nano Lett.*, 2015, **15**, 5635–5640.
16 H.-W. Chen, J.-H. Lee, B.-Y. Lin, S. Chen and S.-T. Wu, Liquid crystal display and organic light-emitting diode display: present status and future perspectives, *Light: Sci. Appl.*, 2018, **7**, 17168.
17 V. Wood and V. Bulović, Colloidal quantum dot light-emitting devices, *Nano Rev.*, 2010, **1**, 5202.
18 S. Seo, M. R. Gartia and G. L. Liu, Vertically stacked plasmonic nanoparticles in a circular arrangement: a key to colorimetric refractive index sensing, *Nanoscale*, 2014, **6**, 11795–11802.
19 R. C. Somers, M. G. Bawendi and D. G. Nocera, CdSe nanocrystal based chem-/bio- sensors, *Chem. Soc. Rev.*, 2007, **36**, 579–591.
20 B. Adhikari and A. Banerjee, Facile Synthesis of Water-Soluble Fluorescent Silver Nanoclusters and HgII Sensing, *Chem. Mater.*, 2010, **22**, 4364–4371.
21 A. Albanese, P. S. Tang and W. C. Chan, The effect of nanoparticle size, shape, and surface chemistry on biological systems, *Annu. Rev. Biomed. Eng.*, 2012, **14**, 1–16.
22 S. Mitragotri, D. G. Anderson, X. Chen, E. K. Chow, D. Ho, A. V. Kabanov, J. M. Karp, K. Kataoka, C. A. Mirkin, S. H. Petrosko, J. Shi, M. M. Stevens, S. Sun, S. Teoh, S. S. Venkatraman, Y. Xia, S. Wang, Z. Gu and C. Xu, Accelerating the Translation of Nanomaterials in Biomedicine, *ACS Nano*, 2015, **9**, 6644–6654.
23 L. Shang, K. Nienhaus and G. U. Nienhaus, Engineered nanoparticles interacting with cells: size matters, *J. Nanobiotechnol.*, 2014, **12**, 5.
24 F. Lu, S.-H. Wu, Y. Hung and C.-Y. Mou, Size Effect on Cell Uptake in Well-Suspended, Uniform Mesoporous Silica Nanoparticles, *Small*, 2009, **5**, 1408–1413.
25 Y. Shu, L. Sun, Y. Wang, D. Jin, Q. Xu and X. Hu, Polymer surface ligand and silica coating induced highly stable perovskite nanocrystals with enhanced aqueous fluorescence for efficient Hg2+ and glutathione detection, *Analyst*, 2021, **146**, 6798–6807.
26 J. Guo, S. Ye, J. Song and J. Qu, Large-scale synthesis of cesium lead halide perovskite nanocrystals for zinc ion detection, *J. Nanopart. Res.*, 2020, **22**, 153.
27 J. K. George, V. V. Halali, C. G. Sanjayan, V. Suvina, M. Sakar and R. G. Balakrishna, Perovskite nanomaterials as optical and electrochemical sensors, *Inorg. Chem. Front.*, 2020, **7**, 2702–2725.
28 S. Ray, A. Mohapatra and S. Bhaumik, Synthesis of highly stable double-coated Zn-doped cesium lead bromide

nanocrystals for indium ion detection in water, *Mater. Adv.*, 2022, **3**, 4684–4692.

29 X. Sheng, Y. Liu, Y. Wang, Y. Li, X. Wang, X. Wang, Z. Dai, J. Bao and X. Xu, Cesium Lead Halide Perovskite Quantum Dots as a Photoluminescence Probe for Metal Ions, *Adv. Mater.*, 2017, **29**, 1700150.

30 Q. Li, W. Zhou, L. Yu, S. Lian and Q. Xie, Perovskite quantum dots as a fluorescent probe for metal ion detection in aqueous solution via phase transfer, *Mater. Lett.*, 2021, **282**, 128654.

31 Y. Liu, X. Tang, T. Zhu, M. Deng, I. P. Ikechukwu, W. Huang, G. Yin, Y. Bai, D. Qu, X. Huang and F. Qiu, All-inorganic CsPbBr3 perovskite quantum dots as a photoluminescent probe for ultrasensitive Cu2+ detection, *J. Mater. Chem. C*, 2018, **6**, 4793–4799.

32 S. Premkumar, Z. Jin, D. Liu, D. Nataraj, B. B. Mamba, A. T. Kuvarega and J. Gui, Ag2BiI5 Perovskite Quantum Dots Passivated with Oleylamine Sulfide for Solar Cells and Detection of Cu(II) Ions, *ACS Appl. Nano Mater.*, 2021, **4**, 9895–9903.

33 C. Ma, M.-F. Lo and C.-S. Lee, Stabilization of organometallic halide perovskite nanocrystals in aqueous solutions and their applications in copper ion detection, *Chem. Commun.*, 2018, **54**, 5784–5787.

34 N. Ding, D. Zhou, G. Pan, W. Xu, X. Chen, D. Li, X. Zhang, J. Zhu, Y. Ji and H. Song, Europium-Doped Lead-Free Cs3Bi2Br9 Perovskite Quantum Dots and Ultrasensitive Cu2+ Detection, *ACS Sustainable Chem. Eng.*, 2019, **7**, 8397–8404.

35 X. Wu, S. Hu, H. Shao, L. Li, W. Chen, B. Dong, L. Xu, W. Xu, D. Zhou, Z. Wu, H. Song and X. Bai, Introducing ytterbium acetate to luminescent CsPbCl3 nanocrystals for enhanced sensitivity of Cu2+ detection, *Inorg. Chem. Front.*, 2022, **9**, 44–50.

36 H. Huang, M. I. Bodnarchuk, S. V. Kershaw, M. V. Kovalenko and A. L. Rogach, Lead Halide Perovskite Nanocrystals in the Research Spotlight: Stability and Defect Tolerance, *ACS Energy Lett.*, 2017, **2**, 2071–2083.

37 D. Yang, X. Li and H. Zeng, Surface Chemistry of All Inorganic Halide Perovskite Nanocrystals: Passivation Mechanism and Stability, *Adv. Mater. Interfaces*, 2018, **5**, 1701662.

38 S. Bhaumik, S. A. Veldhuis, Y. F. Ng, M. Li, S. K. Muduli, T. C. Sum, B. Damodaran, S. Mhaisalkar and N. Mathews, Highly stable, luminescent core–shell type methylammonium–octylammonium lead bromide layered perovskite nanoparticles, *Chem. Commun.*, 2016, **52**, 7118–7121.

39 G. H. Ahmed, J. Yin, O. M. Bakr and O. F. Mohammed, Successes and Challenges of Core/Shell Lead Halide Perovskite Nanocrystals, *ACS Energy Lett.*, 2021, **6**, 1340–1357.

40 M. R. Kar, S. Ray, B. K. Patra and S. Bhaumik, State of the art and prospects of metal halide perovskite core@shell nanocrystals and nanocomposites, *Mater. Today Chem.*, 2021, **20**, 100424.

41 P. V. Kamat, N. Pradhan, K. Schanze, P. S. Weiss, J. Buriak, P. Stang, T. W. Odom and G. Hartland, Challenges and Opportunities in Designing Perovskite Nanocrystal Heterostructures, *ACS Energy Lett.*, 2020, **5**, 2253–2255.

42 Y. Liu, F. Li, Q. Liu and Z. Xia, Synergetic Effect of Post-synthetic Water Treatment on the Enhanced Photoluminescence and Stability of CsPbX3 (X = Cl, Br, I) Perovskite Nanocrystals, *Chem. Mater.*, 2018, **30**, 6922–6929.

43 V. K. Ravi, S. Saikia, S. Yadav, V. V. Nawale and A. Nag, CsPbBr3/ZnS Core/Shell Type Nanocrystals for Enhancing Luminescence Lifetime and Water Stability, *ACS Energy Lett.*, 2020, **5**, 1794–1796.

44 Z.-J. Li, E. Hofman, J. Li, A. H. Davis, C.-H. Tung, L.-Z. Wu and W. Zheng, Photoelectrochemically Active and Environmentally Stable CsPbBr3/TiO2 Core/Shell Nanocrystals, *Adv. Funct. Mater.*, 2018, **28**, 1704288.

45 G. Jiang, C. Guhrenz, A. Kirch, L. Sonntag, C. Bauer, X. Fan, J. Wang, S. Reineke, N. Gaponik and A. Eychmüller, Highly Luminescent and Water-Resistant CsPbBr3–CsPb2Br5 Perovskite Nanocrystals Coordinated with Partially Hydrolyzed Poly(methyl methacrylate) and Polyethylenimine, *ACS Nano*, 2019, **13**, 10386–10396.

46 H. Wu, Y. Chen, W. Zhang, M. S. Khan and Y. Chi, Water-Dispersed Perovskite Nanocube@SiO2-C18-PC Core–Shell Nanoparticles for Cell Imaging, *ACS Appl. Nano Mater.*, 2021, **4**, 11791–11800.

47 S. N. Raja, Y. Bekenstein, M. A. Koc, S. Fischer, D. Zhang, L. Lin, R. O. Ritchie, P. Yang and A. P. Alivisatos, Encapsulation of Perovskite Nanocrystals into Macroscale Polymer Matrices: Enhanced Stability and Polarization, *ACS Appl. Mater. Interfaces*, 2016, **8**, 35523–35533.

48 M. R. Kar, R. Chakraborty, U. Patel, R. Chakraborty, S. Ray, T. K. Acharya, C. Goswami and S. Bhaumik, Impact of Zn-doping on the composition, stability, luminescence properties of silica coated all-inorganic cesium lead bromide nanocrystals and their biocompatibility, *Mater. Today Chem.*, 2022, **23**, 100753.

49 J. Cai, K. Gu, Y. Zhu, J. Zhu, Y. Wang, J. Shen, A. Trinchi, C. Li and G. Wei, Highly stable CsPbBr3@SiO2 nanocomposites prepared via confined condensation for use as a luminescent ink, *Chem. Commun.*, 2018, **54**, 8064–8067.

50 C. Jia, H. Li, X. Meng and H. Li, CsPbX3/Cs4PbX6 core/shell perovskite nanocrystals, *Chem. Commun.*, 2018, **54**, 6300–6303.

51 B. Wang, C. Zhang, S. Huang, Z. Li, L. Kong, L. Jin, J. Wang, K. Wu and L. Li, Postsynthesis Phase Transformation for CsPbBr3/Rb4PbBr6 Core/Shell Nanocrystals with Exceptional Photostability, *ACS Appl. Mater. Interfaces*, 2018, **10**, 23303–23310.

52 H. Kim, J. H. Park, K. Kim, D. Lee, M. H. Song and J. Park, Highly Emissive Blue Quantum Dots with Superior Thermal Stability via In Situ Surface Reconstruction of Mixed CsPbBr3–Cs4PbBr6 Nanocrystals, *Adv. Sci.*, 2021, 2104660.

53 H. Zhang, X. Wang, Q. Liao, Z. Xu, H. Li, L. Zheng and H. Fu, Embedding Perovskite Nanocrystals into a Polymer Matrix for Tunable Luminescence Probes in Cell Imaging, *Adv. Funct. Mater.*, 2017, **27**, 1604382.

54 Y. Wang, L. Varadi, A. Trinchi, J. Shen, Y. Zhu, G. Wei and C. Li, Spray-Assisted Coil–Globule Transition for Scalable

Preparation of Water-Resistant CsPbBr3@PMMA Perovskite Nanospheres with Application in Live Cell Imaging, *Small*, 2018, **14**, 1803156.

55 B. Huang, F. Chen, Y. Shen, K. Qian, Y. Wang, C. Sun, X. Zhao, B. Cui, F. Gao, Z. Zeng and H. Cui, Advances in Targeted Pesticides with Environmentally Responsive Controlled Release by Nanotechnology, *Nanomaterials*, 2018, **8**, 102.

56 D. Niu, Y. Li and J. Shi, Silica/organosilica cross-linked block copolymer micelles: a versatile theranostic platform, *Chem. Soc. Rev.*, 2017, **46**, 569–585.

57 Y. Ma, S. Liu, H. Yang, Y. Wu, H. Sun, J. Wang, Q. Zhao, F. Li and W. Huang, A water-soluble phosphorescent polymer for time-resolved assay and bioimaging of cysteine/homocysteine, *J. Mater. Chem. B*, 2013, **1**, 319–329.

58 Y. Liu, L. Zhang, X. Long, P. Jiang, C. Geng and S. Xu, Ultrastable CsPbBr3 nanocrystals with lead-carboxylate/SiO2 encapsulation for LED applications, *J. Mater. Chem. C*, 2021, **9**, 12581–12589.

59 Q. Zhong, M. Cao, H. Hu, D. Yang, M. Chen, P. Li, L. Wu and Q. Zhang, One-Pot Synthesis of Highly Stable CsPbBr3@SiO2 Core–Shell Nanoparticles, *ACS Nano*, 2018, **12**, 8579–8587.

60 M. Yang, H.-S. Peng, F.-L. Zeng, F. Teng, Z. Qu, D. Yang, Y.-Q. Wang, G.-X. Chen and D.-W. Wang, In situ silica coating-directed synthesis of orthorhombic methylammonium lead bromide perovskite quantum dots with high stability, *J. Colloid Interface Sci.*, 2018, **509**, 32–38.

61 J. De Roo, M. Ibáñez, P. Geiregat, G. Nedelcu, W. Walravens, J. Maes, J. C. Martins, I. Van Driessche, M. V. Kovalenko and Z. Hens, Highly Dynamic Ligand Binding and Light Absorption Coefficient of Cesium Lead Bromide Perovskite Nanocrystals, *ACS Nano*, 2016, **10**, 2071–2081.

62 Y. Wang, D. Yu, Z. Wang, X. Li, X. Chen, V. Nalla, H. Zeng and H. Sun, Solution-Grown CsPbBr3/Cs4PbBr6 Perovskite Nanocomposites: Toward Temperature-Insensitive Optical Gain, *Small*, 2017, **13**, 1701587.

63 S. Bhaumik, Exciton Relaxation Dynamics in Perovskite Cs4PbBr6 Nanocrystals, *ACS Omega*, 2020, **5**, 22299–22304.

64 L. Ruan, W. Shen, A. Wang, A. Xiang and Z. Deng, Alkyl-Thiol Ligand-Induced Shape- and Crystalline Phase-Controlled Synthesis of Stable Perovskite-Related CsPb2Br5 Nanocrystals at Room Temperature, *J. Phys. Chem. Lett.*, 2017, **8**, 3853–3860.

65 D. Xu, Q. Wan, S. Wu, Y. Zhao, X. Xu, L. Li and G. He, Enhancing the performance of LARP-synthesized CsPbBr3 nanocrystal LEDs by employing a dual hole injection layer, *RSC Adv.*, 2020, **10**, 17653–17659.

66 I. G. Yu, Y. J. Kim, H. J. Kim, C. Lee and W. I. Lee, Size-dependent light-scattering effects of nanoporous TiO2 spheres in dye-sensitized solar cells, *J. Mater. Chem.*, 2011, **21**, 532–538.

67 H. Xu, X. Chen, S. Ouyang, T. Kako and J. Ye, Size-Dependent Mie's Scattering Effect on TiO2 Spheres for the Superior Photoactivity of H2 Evolution, *J. Phys. Chem. C*, 2012, **116**, 3833–3839.

68 A. Sahu, N. Kasoju and U. Bora, Fluorescence Study of the Curcumin–Casein Micelle Complexation and Its Application as a Drug Nanocarrier to Cancer Cells, *Biomacromolecules*, 2008, **9**, 2905–2912.

69 J. C. Yu, J. H. Park, S. Y. Lee and M. H. Song, Effect of perovskite film morphology on device performance of perovskite light-emitting diodes, *Nanoscale*, 2019, **11**, 1505–1514.

70 W. Xiang and W. Tress, Review on Recent Progress of All-Inorganic Metal Halide Perovskites and Solar Cells, *Adv. Mater.*, 2019, **31**, 1902851.

71 S. A. Veldhuis, P. P. Boix, N. Yantara, M. Li, T. C. Sum, N. Mathews and S. G. Mhaisalkar, Perovskite Materials for Light-Emitting Diodes and Lasers, *Adv. Mater.*, 2016, **28**, 6804–6834.

72 D. Cortecchia, J. Yin, A. Petrozza and C. Soci, White light emission in low-dimensional perovskites, *J. Mater. Chem. C*, 2019, **7**, 4956–4969.

73 X. Hou, R. Zhang and D. Fang, Novel whisker-reinforced Al2O3–SiO2 aerogel composites with ultra-low thermal conductivity, *Ceram. Int.*, 2017, **43**, 9547–9551.

74 S. He, G. Sun, X. Cheng, H. Dai and X. Chen, Nanoporous SiO2 grafted aramid fibers with low thermal conductivity, *Compos. Sci. Technol.*, 2017, **146**, 91–98.

75 P. Wu, T. Zhao, S. Wang and X. Hou, Semicondutor quantum dots-based metal ion probes, *Nanoscale*, 2014, **6**, 43–64.

76 V.-G. Margarita and C.-C. Carolina, Analytical strategies based on quantum dots for heavy metal ions detection, *J. Biomed. Opt.*, 2014, **19**, 101503.

77 Y. Lou, Y. Zhao, J. Chen and J.-J. Zhu, Metal ions optical sensing by semiconductor quantum dots, *J. Mater. Chem. C*, 2014, **2**, 595–613.

78 L.-J. Fan, Y. Zhang, C. B. Murphy, S. E. Angell, M. F. L. Parker, B. R. Flynn and W. E. Jones, Fluorescent conjugated polymer molecular wire chemosensors for transition metal ion recognition and signaling, *Coord. Chem. Rev.*, 2009, **253**, 410–422.

79 L. Prodi, M. Montalti, N. Zaccheroni, J. S. Bradshaw, R. M. Izatt and P. B. Savage, Characterization of 5-chloro-8-methoxyquinoline appended diaza-18-crown-6 as a chemosensor for cadmium, *Tetrahedron Lett.*, 2001, **42**, 2941–2944.

80 Y. Ding, S. Z. Shen, H. Sun, K. Sun and F. Liu, Synthesis of l-glutathione-capped-ZnSe quantum dots for the sensitive and selective determination of copper ion in aqueous solutions, *Sens. Actuators, B*, 2014, **203**, 35–43.

81 M. R. Awual, M. Ismael, T. Yaita, S. A. El-Safty, H. Shiwaku, Y. Okamoto and S. Suzuki, Trace copper(II) ions detection and removal from water using novel ligand modified composite adsorbent, *Chem. Eng. J.*, 2013, **222**, 67–76.

82 H. Cho, J. B. Chae and C. Kim, A thiophene-based blue-fluorescent emitting chemosensor for detecting indium(III) ion, *Inorg. Chem. Commun.*, 2018, **97**, 171–175.